APPLIED PHYSICS

# Ultrafast extreme rejuvenation of metallic glasses by shock compression

G. Ding[1,2], C. Li[1,3], A. Zaccone[4,5,6], W. H. Wang[7]*, H. C. Lei[8], F. Jiang[2], Z. Ling[1], M. Q. Jiang[1,3]*



**Structural rejuvenation of glasses not only provides fundamental insights into their complicated dynamics but also extends their practical applications. However, it is formidably challenging to rejuvenate a glass on very short time scales. Here, we present the first experimental evidence that a specially designed shock compression technique can rapidly rejuvenate metallic glasses to extremely high-enthalpy states within a very short time scale of about 365 ± 8 ns. By controlling the shock stress amplitude, the shock-induced rejuvenation is successfully frozen at different degrees. The underlying structural disordering is quantitatively characterized by the anomalous boson heat capacity peak of glasses. A Deborah number, defined as a competition of time scales between the net structural disordering and the applied loading, is introduced to explain the observed ultrafast rejuvenation phenomena of metallic glasses.**

## INTRODUCTION

Time is a critical parameter for characterizing the metastable nature of glasses. The life cycle of glasses is closely associated with time. They are "born" upon cooling glass-forming liquids fast enough to avoid crystal nucleation (*1*) and will age with time via hierarchical dynamic relaxations (*2*, *3*), eventually going toward "death" with full crystallization. Intriguingly, as-quenched or aged glasses can structurally rejuvenate with external energy injection. This process, the inverse of physical aging, also depends on time allowing for configurational excitations across a complex potential energy landscape (PEL). Recently, glass rejuvenation, especially the rejuvenation of metallic glasses, has captured increasing attention due to its scientific and engineering significance (*4*–*8*).

For metallic glasses, structural rejuvenation can be achieved by reheating and faster quenching (*9*), thermal cycling (*4*), elastostatic loading (*10*), thermomechanical creep (*7*, *11*), heavy plastic deformation (*8*, *12*, *13*), etc. Their mechanical and physical properties have been effectively tailored through these rejuvenation strategies (*6*, *14*), expanding their applicability. Usually, the degree of rejuvenation can be quantified by an increase in effective fictive temperature or relaxation enthalpy upon heating. In terms of PEL (*1*), glass rejuvenation represents dynamic hops of a system from deep "strong" basins to shallow "fragile" ones. The underlying mechanism is nonaffine atomic displacements or strains driven by applied stress (*13*, *15*). Using high-energy x-ray diffraction (XRD), Dmowski and co-workers (*5*, *7*, *11*, *13*) have revealed that atomic strains contributing to structural rejuvenation is mainly anelastic and the anelastic strain takes place via complex local rearrangements in the atomic connectivity network from atomic to nanometer length scales.

There is a natural competition between rejuvenation (disordering) and aging (ordering). This is because, in metastable glasses, aging is spontaneous (*3*, *16*) and sometimes can be accelerated by proper thermomechanical processing (*17*, *18*). Once it is balanced with the aging dynamics, structural disordering will be saturated (*19*), and thus rejuvenation ceases to further develop (*5*). For deformation-induced rejuvenation, glasses are usually subjected to a long-time loading with a stress below its yielding point but beyond a threshold (*7*), which effectively activates anelastic atomic strain and simultaneously avoids the acceleration of aging. However, theoretical models based on the free volume (*20*) or shear transformation (ST) (*21*) concept predict that faster loadings or higher strain rates speed up the dynamic process for structural disordering (*19*, *22*). Thus, highly rejuvenated glasses could be accessible in this situation, since there is not enough time for aging to operate. Recently, this prediction has been validated experimentally but within the quasi-static strain-rate range (*5*). With further increasing strain rate, higher-level structural disordering is prone to localization into shear bands with ~10-nm thickness (*23*–*25*). This extreme spatial instability, in turn, reduces the extent of rejuvenation throughout the entire sample. Naturally, a question arises: Is it possible to achieve rejuvenation of glasses at very short loading time scale but without interference from shear banding? So far, there is no experimental evidence to address this challenging question.

In this work, with a specially designed self-unloading double-target technique (*26*), the extreme rejuvenation of a bulk metallic glass is successfully achieved in the, to date, shortest time scale of about 365 ns, while without the introduction of shear bands. The atomic mechanism for the observed ultrafast rejuvenation points to the ST-type atomic rearrangements, as revealed previously (*5*, *7*, *11*, *13*). Here, using low-temperature heat capacity measurements and theoretical analysis of boson peaks (BPs), we demonstrate how nanocale STs induce the glass rejuvenation in terms of excess relaxation enthalpy. Furthermore, from the perspective of time scales, we propose a Deborah number to explain why the ultrafast rejuvenation takes place within a very short time window. Our work provides solid evidence for the possibility of ultrafast rejuvenation of metallic glasses and also increases the understanding of atomic mechanism behind glass rejuvenation.

## RESULTS

### Self-unloading shock compression technique

We use a light-gas gun facility to conduct plate impact experiments with a specially designed flyer target configuration, as schematized

[1]State Key Laboratory of Nonlinear Mechanics, Institute of Mechanics, Chinese Academy of Sciences, Beijing 100190, China. [2]State Key Laboratory for Mechanical Behavior of Materials, Xi'an Jiaotong University, Xi'an 710049, China. [3]School of Engineering Science, University of Chinese Academy of Sciences, Beijing 100049, China. [4]Department of Physics, University of Milan, via Celoria 16, Milano 20133, Italy. [5]Department of Chemical Engineering and Biotechnology, University of Cambridge, Cambridge CB2 3RA, UK. [6]Cavendish Laboratory, University of Cambridge, Cambridge CB3 9HE, UK. [7]Institute of Physics, Chinese Academy of Sciences, Beijing 100190, China. [8]Department of Physics, Renmin University of China, Beijing 100872, China.
*Corresponding author. Email: mqjiang@imech.ac.cn (M.Q.J.); whw@iphy.ac.cn (W.H.W.)

in Fig. 1A. The bulk metallic glass is adopted as both flyer and target materials. The target is separated two parallel touching plates (front and back). Such a double-target technique was previously developed to study the dynamic damage of the back target (*26*). In this work, however, we focus on rejuvenation of the front target. Driven by a projectile, the flyer impacts the front target at an initial velocity $V_0$. Further information on the experiment is available in Materials and Methods. Figure 1B is the *t*-*X* (time versus distance) diagram that illustrates how a stress wave propagates in the flyer and targets during a typical plate impact experiment. Before impact, both flyer and targets reside in a static, stress-free state (0). Upon impact, a forward compressive wave $C_1$ and a backward compressive wave $C_2$ are generated simultaneously and then propagate into the targets and the flyer, respectively. Because of the $C_1$, the front and back targets successively enter a compressive stress state (*2*). For the front target, the duration $\Delta t$ of the state (*2*) is determined by the release (unloading) wave $R_2$ that is the reflection of $C_2$ at the free surface of the flyer. The $C_1$ also reflects a release wave $R_1$ at the free surface of the back target. The interaction of the $R_1$ and $R_2$ brings the back target into a tensile stress state (*5*) where a spallation may well take place (*27*, *28*). Such a stress wave technique allows the front target to undergo a shock compression ($C_1$) and sudden self-unloading ($R_2$). The front target, except for the region close to its free edge, resides in a one-dimensional (1D) strain and a triaxial stress state (see section S2). Therefore, the $C_1$ propagates approximately in 1D with a strong circumferential constraint of deformation. These strategies rule out the possibility of the shear band instability in the front target where the metallic glass is expected to deform homogeneously. According to the Hugoniot data of this glass (*29*), the duration $\Delta t$ of the compressive wave $C_1$ is almost fixed to be less than 400 ns, but the stress amplitude $\sigma_p$ of the $C_1$ depends on the particle velocity (PV) in state (*2*).

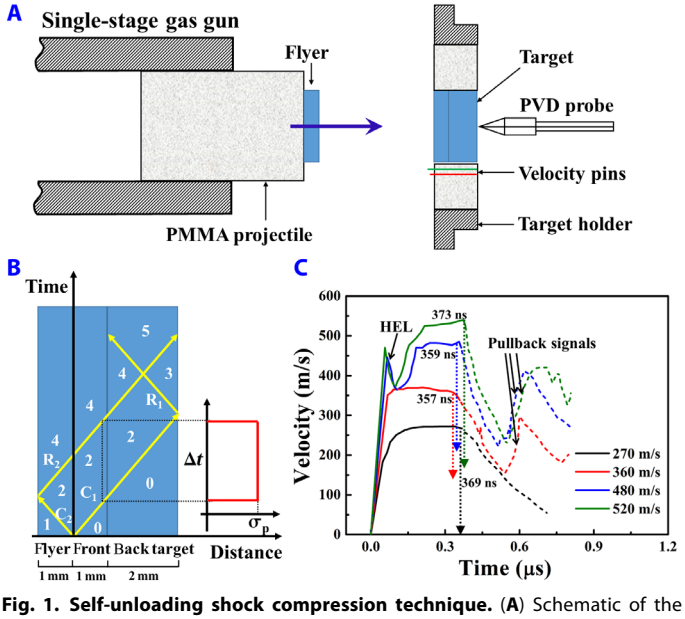


**Fig. 1. Self-unloading shock compression technique.** (**A**) Schematic of the light-gas gun-driven plate impact experimental configuration. PMMA, poly(methyl methacrylate). (**B**) Time versus distance diagram that illustrates the stress wave propagation in the flyer and targets. (**C**) FSV history of the front (solid lines) and back (solid + dashed lines) targets under different initial impact velocities of the flyer. Hugoniot elastic limit (HEL) is the dynamic yield strength of materials.

With the developed technique, four plate impact experiments were performed at initial impact velocities $V_0$ = 270, 360, 480, and 520 m/s, respectively. The nominal strain rate correspondingly ranges from $2.7 \times 10^5$ to $5.2 \times 10^5$ $s^{-1}$. For each impact, the time evolution of PV in the targets can be obtained by measuring the free-surface velocity (FSV) of the back target, which is shown in Fig. 1C. Following the impact, the front and back targets have the same wave profile until the former rapidly separates from the latter because of the unloading effect of the release wave $R_2$ (Fig. 1B). Therefore, the front target only experiences a plateau-shape PV history (the solid lines), while the back target is subjected to the entire shock process (the solid and dashed lines). As designed, a sudden compression-and-unloading process is satisfactorily achieved in the front target where no PV signals of shear banding are detected. The absence of shear banding is also evidenced by the estimated shock strain with relatively small values (see table S1). The duration $\Delta t$ of the compression wave $C_1$ is measured to be about 365 ± 8 ns, within the experimental error range. Depending on the plateau values ($\approx V_0$), the amplitudes $\sigma_p$ of the $C_1$ are calculated to be about 4.33, 5.78, 7.71, and 8.35 GPa. With increasing $V_0$ or $\sigma_p$, the PV profile changes from the single-wave to the typical two-wave structure across a Hugoniot elastic limit (HEL) of about 7.16 GPa. This indicates a transition from the elastic to elastoplastic deformation of the targets, permitting one to examine the ultrafast rejuvenation of a glass across its dynamic yielding. Moreover, at $V_0$ = 360, 480, and 520 m/s, we observed the "pullback" behaviors in the PV profiles of the back target, which is the typical signal of the spallation damage (*27*, *28*) but beyond the focus of this study.

## Ultrafast extreme rejuvenation of metallic glasses

For the front targets after shock compression, the rejuvenation extent of metallic glasses is quantified in terms of their excess relaxation enthalpy $\Delta H_{rel}$ before the glass transition. As shown in Fig. 2A, the $\Delta H_{rel}$ of 0.423 kJ/mol in the as-cast glass remarkably increases by about 68 to 212% to 0.712 to 1.321 kJ/mol in the shock-compressed ones. The higher the impact velocity $V_0$ or the shock stress $\sigma_p$ is, the larger the $\Delta H_{rel}$ of the rejuvenated glasses (Fig. 2B). There is a more rapid increase of the $\Delta H_{rel}$ across the HEL, implying that the global dynamic yielding is more conducive to glass rejuvenation. The observed rejuvenation jump is expected to be mainly induced by anelastic deformation, where the adiabatic heating due to plasticity should play a minor role. This is evidenced by the direct correlation between the estimated shock strain and the $\Delta H_{rel}$ (see fig. S2), consistent with Fig. 2B. The highest $\Delta H_{rel}$ = 1.321 kJ/mol is achieved at $V_0$ = 520 m/s or $\sigma_p$ = 8.35 GPa, which is comparable to the extreme value ($\Delta H_{rel}$ = 1.130 kJ/mol) recently reported by Pan *et al.* (*8*) in a notched Zr-based glass triaxial compressed to 40% nominal strain. An extensive comparison between this study and previous reports (*4*, *8*, *10*, *15*, *30*–*40*) (see table S2) is summarized in Fig. 3 by plotting the $\Delta H_{rel}$ of rejuvenated glasses as a function of the time scale of various rejuvenation methods. Obviously, the present shock compression technique can rejuvenate the glass into an extremely high-enthalpy state when the shock stress $\sigma_p$ exceeds the HEL of glass. Note that this extreme $\Delta H_{rel}$ = 1.321 kJ/mol is still below a few values reported previously (*39*, *40*). We therefore believe that the present glasses could be further rejuvenated to higher $\Delta H_{rel}$ if the impact velocity is further increased. The extreme rejuvenation is achieved within the exceptionally short time scale of 365 ± 8 ns. This time scale is much less than those of other rejuvenation methods by about 10 orders of magnitude.

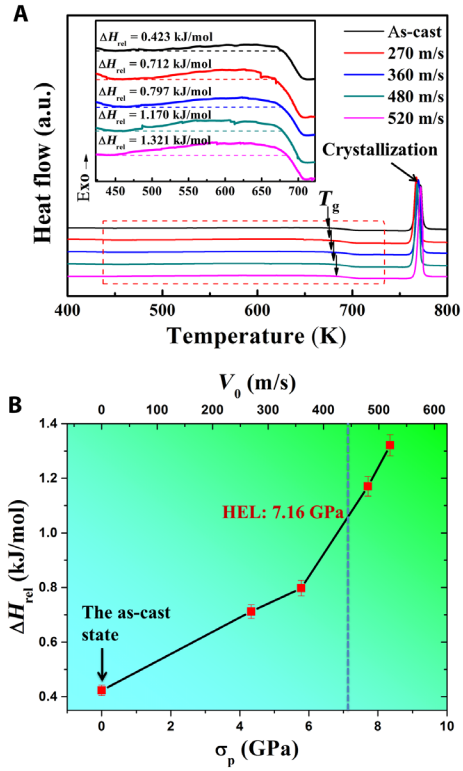


**Fig. 2. Ultrafast extreme rejuvenation of metallic glasses.** (**A**) Differential scanning calorimetry curves. Inset shows the close up of the excess enthalpy of relaxation below $T_g$, i.e., the region highlighted by the dashed rectangle. a.u., arbitrary units. (**B**) Excess relaxation enthalpy versus peak stress (bottom *x* axis) and initial impact velocity (top *x* axis) of the shock compression.

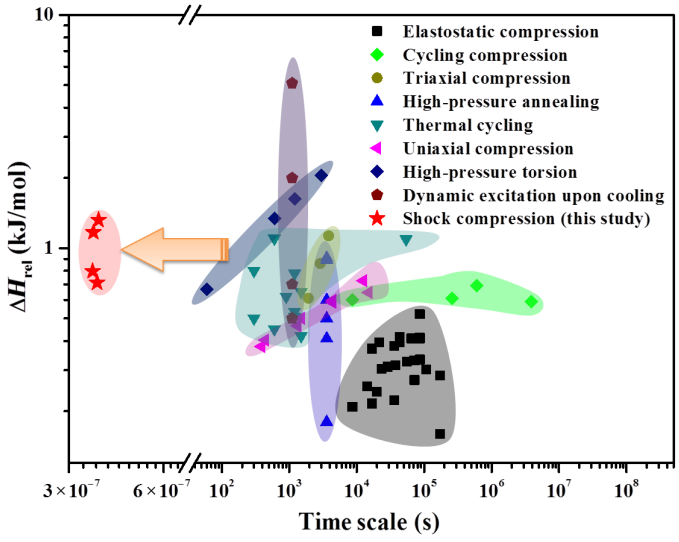


**Fig. 3. Excess relaxation enthalpy of rejuvenated metallic glasses as a function of the time scale of various rejuvenation methods, including shock compression in this study, elastostatic compression (*10*, *15*, *30*–*34*), cycling compression (*35*), triaxial compression (*8*), high-pressure annealing (*36*), thermal cycling (*4*, *37*), uniaxial compression (*38*), high-pressure torsion (*39*), and dynamic excitation upon cooling (*40*).**

## Microstructure of rejuvenated glasses

Figure 4 (A to D) presents the typical high-resolution transmission electron microscopy (HRTEM) images of the ultrafast-rejuvenated glasses at $V_0$ = 270, 360, 480, and 520 m/s, respectively. Long-range disordered, maze-like packing of atoms is observed, which is consistent with the halo ring selected-area electron diffraction (SAED) patterns (insets). Through the quantitative analysis of these SAED patterns (see section S4) (*41*, *42*), we obtain the diffraction intensity profiles $I_{red}(Q)$ for different rejuvenated states (see fig. S3). The first peak position $Q_1$ of $I_{red}(Q)$ indicates the average interatomic spacing (*43*, *44*), which should directly link the atomic free volume in terms of the excess relaxation enthalpy $\Delta H_{rel}$. This is confirmed by the observed inversely linear correlation between the $\Delta H_{rel}$ and the $Q_1$ (see fig. S4). The Fourier transform of the $I_{red}(Q)$ leads to the atomic radial distribution function (RDF) $G(r)$ in real space, as shown in Fig. 4E. This result indicates that the structural disordering behind glass rejuvenation involves complicated atomic rearrangements at length scales extending to nanometers. As compared with the as-cast state, the extremely rejuvenated glasses have a higher concentration of free volume at the atomic scale and simultaneously show larger-size structural disordering at the nanoscale. The multiscale structural disordering can be also indicated by measuring the mechanical hardness of these rejuvenated glasses (see section S5). An inversely linear correlation between the $\Delta H_{rel}$ and the hardness is observed, as shown in fig. S5B.

## Boson heat capacity peak of rejuvenated glasses

The rejuvenated glasses are further characterized by their vibrational dynamics. At terahertz frequencies, disordered glasses universally display an excess of vibrational modes over the Debye level, forming the BP (*45*). These extra vibrations contribute to the enhancement of the low-temperature $T$ specific heat capacity $C_p$ as compared to the Debye $T^3$ law, and thus the BP can be visible as a maximum in the plot of $C_p/T^3$ versus $T$ at temperatures of ~10 K. For metallic glasses, we should subtract the electronic part $C_p^{ele}$ from the low-temperature $C_p$ to make the BP more pronounced. The electronic $C_p^{ele} = \gamma T$, where the Sommerfeld coefficient γ can be determined by a standard procedure (see section S6 for more details) (*46*). Figure 5A plots $(C_p - \gamma T)/T^3$ versus $T$ for the as-cast and shock-induced rejuvenated glasses. The BPs appear as maxima of $(C_p - \gamma T)/T^3$ at ~10 K, showing a positive correlation with the rejuvenation of metallic glasses. With heavier rejuvenation at higher $V_0$, the BP becomes stronger. At the same time, its position $T_{BP}$ moves to lower temperatures and shows an inversely linear correlation with the $\Delta H_{rel}$ (see Fig. 5B).

## DISCUSSION

Using the ad hoc designed plate impact experiments (see Fig. 1), we successfully apply a constrained 1D self-unloading shock compression on the metallic glasses. The duration of the shock is fixed to be about 365 ± 8 ns. The shock stress amplitude ranges from 4.33 to 8.35 GPa across the HEL (7.16 GPa), i.e., the dynamic yield strength of the studied glass. The shock compression can rapidly rejuvenate the as-cast glass into extremely high-enthalpy states, which is controlled by the applied shock stress (see Fig. 2). The ultrafast rejuvenation of glasses is associated not only with the creation of atomic free volume (the increase of $\Delta H_{rel}$) but also the structural rearrangements of atoms occurring at the nanoscale (see Fig. 4). The atomic mechanism revealed

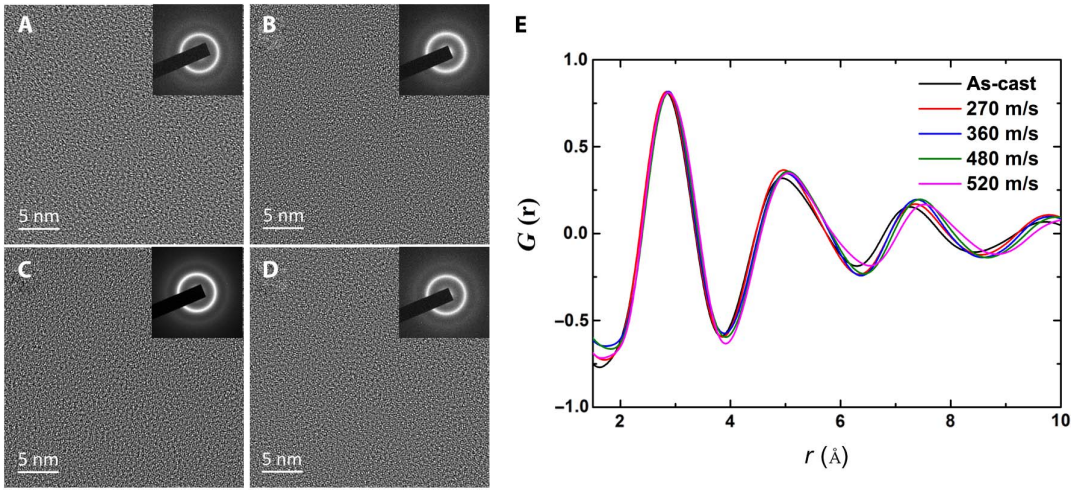


**Fig. 4. Structural characterization of the rejuvenated metallic glasses.** (**A** to **D**) HRTEM images of the rejuvenated states under initial impact velocities of 270, 360, 480, and 520 m/s, respectively. (**E**) RDFs of the as-cast and rejuvenated glasses deduced from the SAED patterns inserted in (A) to (D) and fig. S1B.

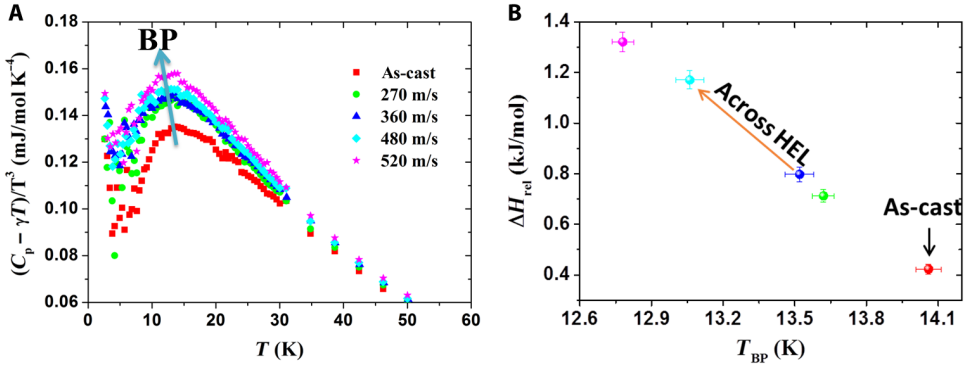


**Fig. 5. BPs of the as-cast and rejuvenated metallic glasses.** (**A**) The plot of $(C_p - \gamma T)/T^3$ versus $T$ in the temperature interval of 2 to 50 K. (**B**) Correlation between the excess relaxation enthalpy and the BP temperature.

here agrees with the finding of Dmowski and co-workers (*5*, *7*, *11*, *13*) that structural changes behind glass rejuvenation involve extensive atomic rearrangements beyond a simple generation of free volume at the atomic scale. The nanoscale structural rearrangements are linked to the action of STs, which can interact with the free volume dynamics (*19*, *22*, *47*).

The measured boson heat capacity peak (Fig. 5) provides a good probe of STs that underpin the glass rejuvenation, in which the frequency $\omega_{BP}$ of BPs is a key parameter. Recent studies (*48*, *49*) have shown that the $\omega_{BP}$ coincides with the Ioffe-Regel (IR) limit of transverse phonons. At this limit, the mean free path of phonons becomes similar to their wavelength $\lambda_{IR}$, causing substantial scattering of the phonons and producing quasi-localized modes to make up the BP. The eigenvectors of BP modes tend to spatially localize in some defective regions where relaxations or STs preferentially take place (*50*–*52*). This explains the observed positive rejuvenation-BP correlation (Fig. 5). Meanwhile, the $\lambda_{IR}$ measures the characteristic size of the quasi-localized modes, which can be estimated as $\lambda_{IR} \approx 2\pi c_T/\omega_{BP}$. The calculation of $\omega_{BP}$ is provided in Materials and Methods. The calculated $\lambda_{IR}$ values range from 1.524 to 1.735 nm (see table S2), depending on the rejuvenation degree of glasses. These values agree well with the characteristic sizes of STs (*53*, *54*), which confirms the ST-related nature of the glass rejuvenation (*5*). Furthermore, we plot the relaxation enthalpy $\Delta H_{rel}$ as a function of the $\lambda_{IR}$, which is shown in Fig. 6A. It is seen that the $\Delta H_{rel}$ increases with $\lambda_{IR}$, indicating that larger-size STs facilitate the creation of atomic free volume during the glass rejuvenation. Such a multiscale structural disordering speeds up across the HEL (i.e., the dynamic yielding strength) of glasses. This is consistent with Fig. 2B.

Last, we introduce a dimensionless Deborah number to study the temporal possibility of the ultrafast rejuvenation of glasses. The Deborah number is defined as (*24*) $De = t_i/t_e$, where $t_i$ stands for the internal structural response time under loading and $t_e$ for the macroscopic imposed time of external loading. The magnitude of De provides a useful indication whether a material behaves in a more fluid-like or solid-like manner. In the present case of the glass rejuvenation, we consider $t_i$ as the characteristic time scale of the underlying structural disordering and $t_e$ as the shock pulse of about 365 ns. In shock experiments, the loading rate effect is reflected by the duration of shock stress, which is very different from the quasi-static or dynamic loading where the rising time of stress or strain is adopted. If $t_i < t_e$, i.e., $De < 1$, then the glass rejuvenation will probably

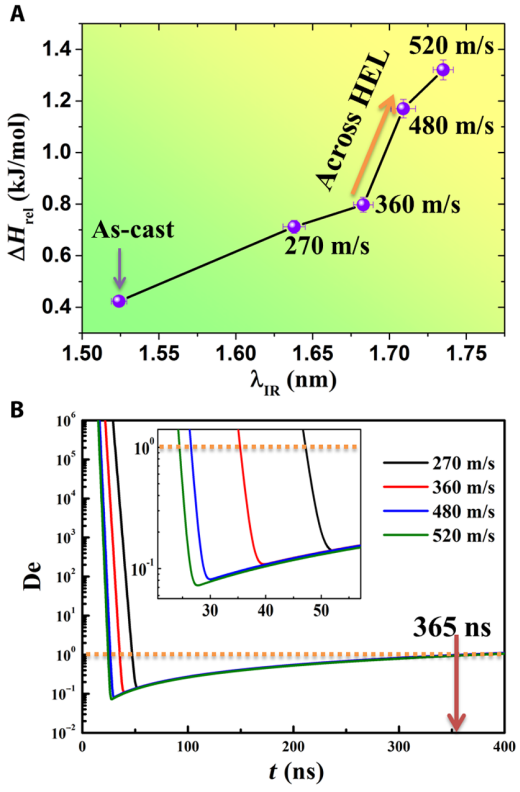


**Fig. 6. Spatiotemporal mechanism for ultrafast extreme rejuvenation of metallic glasses.** (**A**) Relaxation enthalpy $\Delta H_{rel}$ as a function of $\lambda_{IR}$. (**B**) Deborah number De versus loading time at different shock velocities.

take place. However, in the opposite case, i.e., De > 1, there is not enough time for the occurrence of structural rejuvenation. The $t_i$ can be calculated by the Maxwell equation $t_i = \eta/G$, where η is the dynamic viscosity. Under the present high–strain rate loading, the time evolution of η is calculated on the basis of a constitutive model of amorphous plasticity developed previously by Jiang *et al.* (*19*). In this model, the interaction between STs and free volume dynamics is taken into account, which well captures the structural mechanism for the glass rejuvenation. Meanwhile, the decrease of *G* induced by the rejuvenation can be calculated on the basis of the universal evolution of boson heat capacity peaks observed in various metallic glasses (*46*). Figure 6B shows the variations of Deborah number De with loading time at different initial impact velocities. It is found that the De rapidly decreases from a very high value to about 0.1 within several tens of nanoseconds (see inset of Fig. 6B). Higher impact velocities lead to lower De at earlier times, indicating the possibility of faster structural rejuvenations. The underlying mechanism is that, at higher impact velocities, higher levels of stress can be reached faster, which activates STs and free volume creation more rapidly (see fig. S8). After yielding, the structural dynamics slows down, but De < 1 is still satisfied until the end of the shock pulse (~365 ns). The undershoot of De evident in Fig. 6B mirrors the well-known overshoot, which is universally seen in the stress-strain curves of glasses (*19*).

## CONCLUSIONS

In summary, we successfully achieve the ultrafast and extreme rejuvenation of metallic glasses with a specially designed self-unloading shock compression technique. The degree of the glass rejuvenation increases with increasing shock stress at the fixed shock pulse of ~365 ns, showing a surge of relaxation enthalpy across the dynamic yielding of the glass. The rejuvenated metallic glasses are extensively characterized in terms of their thermodynamics, multiscale structures, and vibrational dynamics through boson heat capacity peaks. It is revealed that the nanoscale ST–mediated free volume creation acts as the physical mechanism for the observed shock-induced rejuvenation of metallic glasses. The present results are of significance not only for the understanding of short-time glass dynamics but also for the promising application of metallic glasses in high-velocity impacts.

## MATERIALS AND METHODS

### Material preparation and characterizations

The bulk metallic glass, $Zr_{55}Cu_{30}Ni_5Al_{10}$ (atomic %), in this study was prepared by suction casting from master alloys ingots to a water-cooled copper mold in an arc furnace. The structure of the as-cast glass was confirmed by XRD with Cu Kα radiation and HRTEM (JEM-2100F, JEOL, operated at 200 keV) (see fig. S1). The density ρ of glass was measured to be 6.76 g/cm$^3$ by Archimedean method. The longitudinal and transverse wave speeds ($c_L$ and $c_T$) were determined to be 4750 and 2150 m/s, respectively, via ultrasonic pulse-echo technique. The elastic constants such as shear modulus *G*, Young's modulus *E*, and Poisson's ratio ν can be calculated on the basis of the measured density and wave speeds.

### Plate impact experiment

The 101-mm bore single-stage light-gas gun was used to conduct the plate impact experiments. The schematic of the experimental configuration is shown in Fig. 1A. The flyer and the front and back targets were disk plates with the thicknesses of 1, 1, and 2 mm, respectively, along the shock direction, and their diameter was all 36 mm. A low-impedance poly(methyl methacrylate) project carrying the flyer was driven by the high-pressure nitrogen to impact the front target. The rear end of the projectile had a sealing O-ring and a Teflon key that slid in a key way inside the gun barrel to prevent any rotation of the projectile. A pair of coaxial electric probes was embedded in the epoxy holder of targets to record the initial velocity of impact. Both the flyer and the targets were carefully finished in parallel to ensure the generation of plane waves after normal impact. The stress amplitude of a shock wave can be calculated through the relation $\sigma_p = \rho c_L V_p$, where $V_p$ is the material PV. A photonic Doppler velocimetry system was adopted to measure the FSV ($\approx 2V_p$) of the back target. All targets were soft-recovered by decelerating into several stages of cotton drags. Shear bands or cracks were not observed in the recovered front targets.

### Structural and thermal characterizations

For the post-impact glasses, structural analyses were performed by HRTEM and SAED. The thermal response of glasses was investigated with differential scanning calorimetry (DSC; TA Q2000): heating the glass up to 823 K in a pure argon atmosphere at a heating rate of 20 K/min and subsequent cooling to room temperature at the same rate. The specific heat capacity was measured under high vacuum conditions with a Quantum Design physical property measurement system (PPMS), which allows cooling down to 2 K with a liquid helium system. For comparison, both DSC and PPMS measurements were also performed on the original as-cast glasses.

### Calculation of the BP frequency

The total specific heat capacity $C_p$ of the glass is expressed as

$$C_p = C_p^{ele} + n_D C_p^{Debye} + n_q C_p^{quasi} \quad (1)$$

where $n_D$ and $n_q$ represent the Debye and quasi-localized contributions per mole, respectively. The Debye term $C_p^{Debye}$ is

$$C_p^{Debye} = 9R\left(\frac{T}{\theta_D}\right)^3 \int_0^{\theta_D/T} \frac{\xi^4 e^{\xi}}{(e^E - 1)^2} d\xi \quad (2)$$

where $R$ is the gas constant and $\theta_D$ is the Debye temperature that can be obtained by fitting the $C_p$ data below 8 K (see fig. S6). The quasi-localized term $C_p^{quasi}$ can be written as

$$C_p^{quasi} = 3R\int_0^{\omega^*} \left(\frac{\hbar\omega}{k_B T}\right)^2 \frac{e^{\hbar\omega/k_B T}}{(e^{\hbar\omega/k_B T} - 1)^2} g_q(\omega) d\omega \quad (3)$$

where ħ, $k_B$, and ω are the Planck constant, the Boltzmann constant, and the frequency, respectively. Considering the hybrid nature of quasi-localized and Debye modes (*55*), the upper limit ω* of integral was reasonably chosen as the Debye frequency $\omega_D = k_B\theta_D/\hbar$. The $g_q(\omega)$ is the vibrational density of states or the frequency distribution of the quasi-localized modes, which is the key to determine the $C_p^{quasi}$ and resultant BP. It is well accepted that the spatial heterogeneity of elastic modulus incurs the emergence of quasi-localized modes (*48*, *49*, *56*). Shear modulus and BP intensity are strongly correlated (*46*, *57*). We therefore examined the distribution of elastic modulus in metallic glasses (*58*, *59*) and found that the data can be well fitted by a formula analogous to the Planck's law of black-body radiation. Therefore, we assumed that the quasi-localized modes $g_q(\omega)/\omega^2$ normalized by the Debye law obeys a Planck-like distribution

$$g_q(\omega)/\omega^2 = \frac{\varphi\omega^3}{e^{\ell\omega} - 1} \quad (4)$$

where the parameter $\varphi = 5.572 \times 10^{-15}$ is determined by the high-temperature limit ($3R$) of $C_p$ and the $\ell$ can be determined by the position $T_{BP}$ of the $C_p$-BP. It is noticed that $\lim_{\omega\to 0} g_q(\omega) \sim \omega^4$, which is consistent with the statistic law of low-frequency quasi-localized modes revealed recently (*60*). Uniting Eqs. 1 to 4, both the $C_p$ and $(C_p - \gamma T)/T^3$ data were satisfactorily fitted, and the contributions from the electronic $C_p^{ele}$, the Debye $C_p^{Debye}$, and the quasi-localized vibrational $C_p^{quasi}$ can be calculated, respectively. The results are shown in fig. S7, and all relevant parameters are listed in table S3. According to the measured $T_{BP}$, the frequency $\omega_{BP}$ of BP can be determined by $\partial[g_q(\omega)/\omega^2]/\partial\omega\,|_{\omega_{BP}} = 0$.

## SUPPLEMENTARY MATERIALS

Supplementary material for this article is available at http://advances.sciencemag.org/cgi/content/full/5/8/eaaw6249/DC1

Section S1. Structural characterizations of the as-cast $Zr_{55}Cu_{30}Ni_5Al_{10}$ bulk metallic glass
Section S2. Stress and strain state analysis for the front target
Section S3. Experimental data about rejuvenation of metallic glasses from literature
Section S4. Diffraction profile analysis of SAED patterns
Section S5. Nanoindentation measurements and analyses
Section S6. Determination of the electronic $C_p$ contribution
Section S7. Theoretical fitting of low-temperature heat capacity data
Section S8. Calculations of the constitutive behaviors of metallic glasses
Table S1. The triaxial stress and the 1D strain state in the front target under different impact velocities.
Table S2. Relaxation enthalpy of metallic glasses by various rejuvenation methods.
Table S3. All parameters related to the BP analyses.
Fig. S1. Structural characterizations of the as-cast $Zr_{55}Cu_{30}Ni_5Al_{10}$ bulk metallic glass.
Fig. S2. Correlation between excess relaxation enthalpy and calculated shock strain.
Fig. S3. Diffraction profiles of SAED patterns.
Fig. S4. Correlation between excess relaxation enthalpy and first peak position of reduced diffraction profile.
Fig. S5. Nanoindentation measurements on the as-cast and rejuvenated glasses.
Fig. S6. Determination of the electronic contribution to low-temperature specific heat capacity.
Fig. S7. Theoretical fitting of low-temperature heat capacity data.
Fig. S8. Constitutive responses of the $Zr_{55}Cu_{30}Ni_5Al_{10}$ bulk metallic glass under the present high–strain rate loading.

## REFERENCES AND NOTES


1. P. G. Debenedetti, F. H. Stillinger, Supercooled liquids and the glass transition. *Nature* **410**, 259–267 (2001).
2. H.-B. Yu, R. Richert, K. Samwer, Structural rearrangements governing Johari-Goldstein relaxations in metallic glasses. *Sci. Adv.* **3**, e1701577 (2017).
3. I. Gallino, R. Busch, Relaxation pathways in metallic glasses. *JOM* **69**, 2171–2177 (2017).
4. S. V. Ketov, Y. H. Sun, S. Nachum, Z. Lu, A. Checchi, A. R. Beraldin, H. Y. Bai, W. H. Wang, D. V. Louzguine-Luzgin, M. A. Carpenter, A. L. Greer, Rejuvenation of metallic glasses by non-affine thermal strain. *Nature* **524**, 200–203 (2015).
5. Y. Tong, T. Iwashita, W. Dmowski, H. Bei, Y. Yokoyama, T. Egami, Structural rejuvenation in bulk metallic glasses. *Acta Mater.* **86**, 240–246 (2015).
6. Y. Sun, A. Concustell, A. L. Greer, Thermomechanical processing of metallic glasses: Extending the range of the glassy state. *Nat. Rev. Mater.* **1**, 16039 (2016).
7. Y. Tong, W. Dmowski, H. Bei, Y. Yokoyama, T. Egami, Mechanical rejuvenation in bulk metallic glass induced by thermo-mechanical creep. *Acta Mater.* **148**, 384–390 (2018).
8. J. Pan, Y. X. Wang, Q. Guo, D. Zhang, A. L. Greer, Y. Li, Extreme rejuvenation and softening in a bulk metallic glass. *Nat. Commun.* **9**, 560 (2018).
9. M. Wakeda, J. Saida, J. Li, S. Ogata, Controlled rejuvenation of amorphous metals with thermal processing. *Sci. Rep.* **5**, 10545 (2015).
10. K.-W. Park, C.-M. Lee, M. Wakeda, Y. Shibutani, M. L. Falk, J.-C. Lee, Elastostatically induced structural disordering in amorphous alloys. *Acta Mater.* **56**, 5440–5450 (2008).
11. Y. Tong, W. Dmowski, Y. Yokoyama, G. Wang, P. K. Liaw, T. Egami, Recovering compressive plasticity of bulk metallic glasses by high-temperature creep. *Scripta Mater.* **69**, 570–573 (2013).
12. A. Concustell, F. O. Méar, S. Suriñach, M. D. Baró, A. L. Greer, Structural relaxation and rejuvenation in a metallic glass induced by shot-peening. *Phi. Mag. Lett.* **89**, 831–840 (2009).
13. W. Dmowski, Y. Yokoyama, A. Chuang, Y. Ren, M. Umemoto, K. Tsuchiya, A. Inoue, T. Egami, Structural rejuvenation in a bulk metallic glass induced by severe plastic deformation. *Acta Mater.* **58**, 429–438 (2010).
14. A. L. Greer, Y. H. Sun, Stored energy in metallic glasses due to strains within the elastic limit. *Philos. Mag.* **96**, 1643–1663 (2016).
15. S.-C. Lee, C.-M. Lee, J.-C. Lee, H.-J. Kim, Y. Shibutani, E. Fleury, M. L. Falk, Structural disordering process of an amorphous alloy driven by the elastostatic compression at room temperature. *Appl. Phys. Lett.* **92**, 151906 (2008).
16. C. A. Angell, K. L. Ngai, G. B. McKenna, P. F. McMillan, S. W. Martin, Relaxation in glassforming liquids and amorphous solids. *J. Appl. Phys.* **88**, 3113–3157 (2000).
17. Z. T. Wang, J. Pan, Y. Li, C. A. Schuh, Densification and strain hardening of a metallic glass under tension at room temperature. *Phys. Rev. Lett.* **111**, 135504 (2013).
18. H.-B. Yu, R. Richert, R. Maaß, K. Samwer, Strain induced fragility transition in metallic glass. *Nat. Commun.* **6**, 7179 (2015).
19. M. Q. Jiang, G. Wilde, L. H. Dai, Origin of stress overshoot in amorphous solids. *Mech. Mater.* **81**, 72–83 (2015).
20. F. Spaepen, A microscopic mechanism for steady state inhomogeneous flow in metallic glasses. *Acta Metall.* **25**, 407–415 (1977).
21. A. S. Argon, Plastic deformation in metallic glasses. *Acta Metall.* **27**, 47–58 (1979).
22. J. S. Langer, Dynamics of shear-transformation zones in amorphous plasticity: Formulation in terms of an effective disorder temperature. *Phys. Rev. E Stat. Nonlin. Soft Matter Phys.* **70**, 041502 (2004).
23. M. Q. Jiang, W. H. Wang, L. H. Dai, Prediction of shear-band thickness in metallic glasses. *Scripta Mater.* **60**, 1004–1007 (2009).

24. M. Q. Jiang, L. H. Dai, On the origin of shear banding instability in metallic glasses. *J. Mech. Phys. Solids* **57**, 1267–1292 (2009).
25. A. L. Greer, Y. Q. Cheng, E. Ma, Shear bands in metallic glasses. *Mater. Sci. Eng. R* **74**, 71–132 (2013).
26. X.-Y. Pei, H. Peng, H.-L. He, P. Li, Study on the effect of peak stress on dynamic damage evolution of high pure copper. *Acta Phys. Sin.* **64**, 054601 (2015).
27. J. P. Escobedo, Y. M. Gupta, Dynamic tensile response of Zr-based bulk amorphous alloys: Fracture morphologies and mechanisms. *J. Appl. Phys.* **107**, 123502 (2010).
28. F. Yuan, V. Prakash, J. J. Lewandowski, Spall strength and Hugoniot elastic limit of a zirconium-based bulk metallic glass under planar shock compression. *J. Mater. Res.* **22**, 402–411 (2007).
29. T. Mashimo, H. Togo, Y. Zhang, Y. Uemura, T. Kinoshita, M. Kodama, Y. Kawamura, Hugoniot-compression curve of Zr-based bulk metallic glass. *Appl. Phys. Lett.* **89**, 241904 (2006).
30. S.-J. Lee, B.-G. Yoo, J.-I. Jang, J.-C. Lee, Irreversible structural change induced by elastostatic stress imposed on an amorphous alloy and its influence on the mechanical properties. *Met. Mater. Int.* **14**, 9–13 (2008).
31. S.-C. Lee, C.-M. Lee, J.-W. Yang, J.-C. Lee, Microstructural evolution of an elastostatically compressed amorphous alloy and its influence on the mechanical properties. *Scripta Mater.* **58**, 591–594 (2008).
32. K.-W. Park, C.-M. Lee, M. Wakeda, Y. Shibutani, E. Fleury, J.-C. Lee, Homogeneous deformation of bulk amorphous alloys during elastostatic compression and its packing density dependence. *Scripta Mater.* **59**, 710–713 (2008).
33. J.-C. Lee, Calorimetric study of β-relaxation in an amorphous alloy: An experimental technique for measuring the activation energy for shear transformation. *Intermetallics* **44**, 116–120 (2014).
34. M. Zhang, Y. M. Wang, F. X. Li, S. Q. Jiang, M. Z. Li, L. Liu, Mechanical relaxation-to-rejuvenation transition in a Zr-based bulk metallic glass. *Sci. Rep.* **7**, 625 (2017).
35. D. V. Louzguine-Luzgin, V. Y. Zadorozhnyy, S. V. Ketov, Z. Wang, A. A. Tsarkov, A. L. Greer, On room-temperature quasi-elastic mechanical behaviour of bulk metallic glasses. *Acta Mater.* **129**, 343–351 (2017).
36. C. Wang, Z. Z. Yang, T. Ma, Y. T. Sun, Y. Y. Yin, Y. Gong, L. Gu, P. Wen, P. W. Zhu, Y. W. Long, X. H. Yu, C. Q. Jin, W. H. Wang, H. Y. Bai, High stored energy of metallic glasses induced by high pressure. *Appl. Phys. Lett.* **110**, 111901 (2017).
37. W. Guo, R. Yamada, J. Saida, Rejuvenation and plasticization of metallic glass by deep cryogenic cycling treatment. *Intermetallics* **93**, 141–147 (2018).
38. J. S. Harmon, M. D. Demetriou, W. L. Johnson, M. Tao, Deformation of glass forming metallic liquids: Configurational changes and their relation to elastic softening. *Appl. Phys. Lett.* **90**, 131912 (2007).
39. F. Meng, K. Tsuchiya, S. Il, Y. Yokoyama, Reversible transition of deformation mode by structural rejuvenation and relaxation in bulk metallic glass. *Appl. Phys. Lett.* **101**, 121914 (2012).
40. S. Küchemann, R. Maaß, Gamma relaxation in bulk metallic glasses. *Scripta Mater.* **137**, 5–8 (2017).
41. J. Kim, H. S. Oh, J. Kim, C. W. Ryu, G. W. Lee, H. J. Chang, E. S. Park, Utilization of high entropy alloy characteristics in Er-Gd-Y-Al-Co high entropy bulk metallic glass. *Acta Mater.* **155**, 350–361 (2018).
42. Y. M. Chen, T. Ohkubo, T. Mukai, K. Hono, Structure of shear bands in $Pd_{40}Ni_{40}P_{20}$ bulk metallic glass. *J. Mater. Res.* **24**, 1–9 (2009).
43. A. Slipenyuk, J. Eckert, Correlation between enthalpy change and free volume reduction during structural relaxation of $Zr_{55}Cu_{30}Al_{10}Ni_5$ metallic glass. *Scripta Mater.* **50**, 39–44 (2004).
44. X. Sun, G. Ding, G. Mo, L. H. Dai, M. Q. Jiang, Dilatancy signatures of amorphous plasticity probed by X-ray synchrotron radiation. *Intermetallics* **107**, 34–38 (2019).
45. F. Sette, M. H. Krisch, C. Masciovecchio, G. Ruocco, G. Monaco, Dynamics of glasses and glass-forming liquids studied by inelastic X-ray scattering. *Science* **280**, 1550–1555 (1998).
46. M. Q. Jiang, M. Peterlechner, Y. J. Wang, W. H. Wang, F. Jiang, L. H. Dai, G. Wilde, Universal structural softening in metallic glasses indicated by boson heat capacity peak. *Appl. Phys. Lett.* **111**, 261901 (2017).
47. L. Li, E. R. Homer, C. A. Schuh, Shear transformation zone dynamics model for metallic glasses incorporating free volume as a state variable. *Acta Mater.* **61**, 3347–3359 (2013).
48. S. Gelin, H. Tanaka, A. Lemaître, Anomalous phonon scattering and elastic correlations in amorphous solids. *Nat. Mater.* **15**, 1177–1181 (2016).
49. J. Yang, Y.-J. Wang, E. Ma, A. Zaccone, L. H. Dai, M. Q. Jiang, Structural parameter of orientational order to predict the boson vibrational anomaly in glasses. *Phys. Rev. Lett.* **122**, 015501 (2019).
50. A. Widmer-Cooper, H. Perry, P. Harrowell, D. R. Reichman, Irreversible reorganization in a supercooled liquid originates from localized soft modes. *Nat. Phys.* **4**, 711–715 (2008).
51. M. L. Manning, A. J. Liu, Vibrational modes identify soft spots in a sheared disordered packing. *Phys. Rev. Lett.* **107**, 108302 (2011).
52. J. Ding, S. Patinet, M. L. Falk, Y. Cheng, E. Ma, Soft spots and their structural signature in a metallic glass. *Proc. Natl. Acad. Sci. U.S.A.* **111**, 14052–14056 (2014).
53. M. Zink, K. Samwer, W. L. Johnson, S. G. Mayr, Plastic deformation of metallic glasses: Size of shear transformation zones from molecular dynamics simulations. *Phys. Rev. B* **73**, 172203 (2006).
54. D. Pan, A. Inoue, T. Sakurai, M. W. Chen, Experimental characterization of shear transformation zones for plastic flow of bulk metallic glasses. *Proc. Natl. Acad. Sci. U.S.A.* **105**, 14769–14772 (2008).
55. R. Zorn, The boson peak demystified? *Physics* **4**, 44 (2011).
56. W. Schirmacher, G. Ruocco, T. Scopigno, Acoustic attenuation in glasses and its relation with the boson peak. *Phys. Rev. Lett.* **98**, 025501 (2007).
57. H. Shintani, H. Tanaka, Universal link between the boson peak and transverse phonons in glass. *Nat. Mater.* **7**, 870–877 (2008).
58. Y. Yang, J. F. Zeng, A. Volland, J. J. Blandin, S. Gravier, C. T. Liu, Fractal growth of the dense-packing phase in annealed metallic glass imaged by high-resolution atomic force microscopy. *Acta Mater.* **60**, 5260–5272 (2012).
59. F. C. Li, S. Wang, Q. F. He, H. Zhang, B. A. Sun, Y. Lu, Y. Yang, The stochastic transition from size dependent to size independent yield strength in metallic glasses. *J. Mech. Phys. Solids* **109**, 200–216 (2017).
60. E. Lerner, G. Düring, E. Bouchbinder, Statistics and properties of low-frequency vibrational modes in structural glasses. *Phys. Rev. Lett.* **117**, 035501 (2016).


**Acknowledgments:** We thank L. H. Dai for fruitful discussion. **Funding:** This work was supported by the National Natural Science Foundation of China (grant nos. 11522221 and 11790292), and the Youth Innovation Promotion Association of CAS (grant no. 2013012).
**Author contributions:** M.Q.J. designed and supervised the project. G.D. prepared the materials and performed XRD, DSC, and TEM characterizations. G.D. and C.L. performed the plate impact experiments. G.D. and H.C.L. performed the PPMS measurements. M.Q.J., G.D., C.L., Z.L., W.H.W., F.J., and A.Z. analyzed the data. M.Q.J., G.D., W.H.W., and A.Z. wrote the paper. All authors discussed the results and commented on the manuscript. **Competing interests:** The authors declare that they have no competing interests. **Data and materials availability:** All data needed to evaluate the conclusions in the paper are present in the paper and/or the Supplementary Materials. Additional data related to this paper may be requested from the authors.

Submitted 10 January 2019
Accepted 16 July 2019
Published 23 August 2019
10.1126/sciadv.aaw6249

**Citation:** G. Ding, C. Li, A. Zaccone, W. H. Wang, H. C. Lei, F. Jiang, Z. Ling, M. Q. Jiang, Ultrafast extreme rejuvenation of metallic glasses by shock compression. *Sci. Adv.* **5**, eaaw6249 (2019).